Study of the Multipactor Effect in Ridge Gap Waveguide Technology

Sarah M. Bonte, Manuel Sancho, Ángela Coves, *Senior Member, IEEE*,
Eva Rajo-Iglesias, *Fellow, IEEE*, José J. Vague, and Vicente E. Boria, *Fellow, IEEE*

***Abstract*—Ridge gap waveguides have emerged as promising transmission lines for high-frequency applications and components (i.e. filters), due to their low-loss characteristics and compatibility with standard fabrication processes. This article investigates the limits on the power level (related to the multipactor effect) within ridge gap waveguides, focusing on understanding the distribution and propagation of electromagnetic energy along this waveguide structure. Through simulations, the dependence of power levels on various parameters, such as the ridge dimensions and its proximity to the bed of pins, is explored. Experimental results of the multipactor effect inside a manufactured prototype of a ridge gap waveguide fully validate the simulated data obtained with the available commercial software tools. The insights provided in this research will help the future design and implementation of efficient and reliable high-frequency communication and sensing systems, for space applications, utilizing the ridge gap waveguide technology.**

***Index Terms*—Microwave, multipactor, Ridge Gap Waveguide.**

I. Introduction

MULTIPACTOR (MP) is a well-known and undesired high-power effect frequently observed in microwave and millimeter-wave components operating under high-vacuum conditions [1], which are used in a wide range of different scenarios, such as satellite communication payloads, traveling-wave tubes, as well as particle accelerators. In an ultra-high vacuum environment, the free electrons inside the microwave component are accelerated by the radio frequency (RF) electromagnetic (EM) fields, impacting against its metallic walls and releasing more secondary electrons, giving rise to an avalanche of electrons. Thus, a resonant discharge is produced inside the affected component with a large number of adverse consequences [2]. Among them, it is worth mentioning the detuning of resonant cavities, power dissipation, a significant increase of noise in communication systems, and even physical damages in the involved component.

Over the years, MP susceptibility charts for parallel-plate waveguides (PPW) have been developed using both analytical models [3] and empirical data [4]. The charts are used for approximate prediction of the MP power threshold in different microwave components, either metallic or including dielectric materials [5], [6]. More recently, the MP effect has been explored in a broader range of waveguides and transmission lines, including rectangular [7], [8], ridged [9], [10], circular [11], elliptical [12], and coaxial waveguides [13], [14], as well as planar microstrip lines [15].

In recent years there has been a great development of the gap waveguide technology, a promising alternative to Rectangular Waveguide (RW) technology, due to its potential advantages, mainly because perfect metallic contact between its different parts (top cover and body) is not needed [16]. The emerging Groove Gap Waveguide (GGW) technology, originally proposed in [17], is becoming a promising alternative to replace the standard hollow RW in high-frequency components. Another promising gap waveguide variant is the Ridge Gap Waveguide (RGW) [18], which has become a very useful transmission solution for high-frequency applications, due to its intrinsic low-loss properties and seamless integration into standard fabrication processes. This type of waveguide has been used for the development of efficient and reliable high-frequency communication and sensing systems, especially due to its compact size that makes it ideal for the design of feeding networks and beamforming networks in antenna systems [19]–[21].

There are very few –and recent– contributions addressing the problem of electron discharges in gap waveguide technology so far. In the first one, a study of the MP effect in GGW technology was performed [22], but just considering a very simple E-plane GGW transformer operating on the upper-end side of the X-band (10-12 GHz). The second one is focused on the corona (or gas breakdown) effect in GGWs and inductive bandpass filters based on this technology that, contrary to MP, requires a certain pressure level inside the device [23]. In [24], a theoretical and experimental study of the MP effect in a GGW bandpass filter (and its equivalent RW counterpart) operating in the Ka-band has been fully addressed. However, although MP susceptibility charts have been reported for conventional ridged and multiridged waveguides and applied to different filtering structures [9], [10], there is still a complete lack of theoretical and experimental studies addressing the MP effect in RGW technology. This gap is particularly relevant given the growing use of RGWs in high-frequency and space applications, and it is fully addressed in this article.

This article presents a theoretical and experimental study of the MP threshold levels in RGW technology, whose geometry and design are described in Section II. Next, in Section III, a thorough investigation of the relevant factors that can induce an electron discharge is performed in this waveguide, as well as in other waveguides such as the GGW and the

This work has been funded by the Ministerio de Ciencia, Innovacion y Universidades (Spanish Government) through the Subprojects C41 and C43 of the R&D Projects PID2022-136590OB and project PID2022-141055NB-C22 (under grant AEI/10.13039/501100011033/FEDER, UE).

Sarah M. Bonte, Manuel Sancho, and Ángela Coves are with the Departamento de Ingeniería de Comunicaciones-I3E, Universidad Miguel Hernández de Elche, 03202 Elche, Spain (e-mail: sbonte@umh.es; manuel.sancho@alu.umh.es; angela.coves@umh.es).

Eva Rajo-Iglesias is with the Department of Signal Theory and Communication, Universidad Carlos III de Madrid, 28911 Madrid, Spain (e-mail: eva@tsc.uc3m.es).

José J. Vague and Vicente E. Boria are with the Departamento de Comunicaciones, iTEAM Group, Universitat Politècnica de València, 46022 Valencia, Spain (e-mail: jvague@dcom.upv.es; vboria@dcom.upv.es).

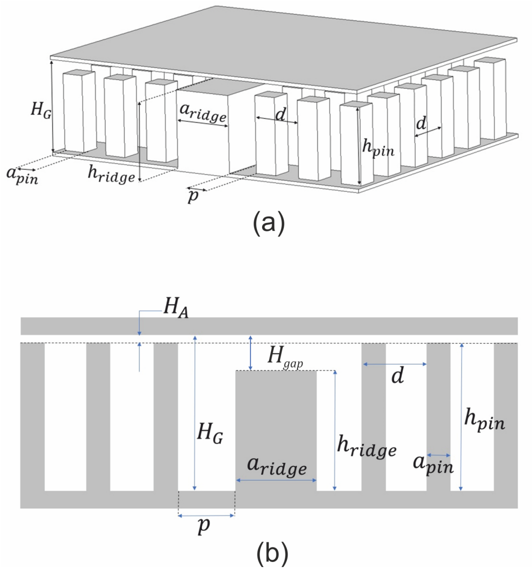

Fig. 1. Geometry of the RGW under study. (a) 3D view and (b) cross-section of the RGW.

standard rectangular waveguide, revealing that RGW technology is much more susceptible to the MP effect, which clearly highlights the relevance of the MP study for such technology. In Section IV, through rigorous simulations, we explore the intricate dependencies of its MP threshold levels on various key parameters, including the ridge dimensions and the distance between the ridge and the first row of pins of the bed of pins. Next, in order to validate the previous theoretical study, an E-plane WR-51 waveguide transformer is designed in Section V, where the central section is implemented in RGW. After that, in Section VI the measured electrical response and the MP threshold levels of this transformer, which has been fabricated in aluminum, are shown to agree well with the simulated data. Finally, the main conclusions of this work are briefly summarized.

II. Geometry and Initial Design

The geometry of the RGW under study can be seen in Figs. 1(a) (3D view) and (b) (cross section), respectively. It is characterized by having a ridge in the central area where the electromagnetic fields will propagate, and beds of pins arranged following a spatial periodicity d. The periodic pins are surrounding the RGW body to provide a high-impedance boundary condition to the top lid (where a small gap of height H_A between pins and top lid is present). As a consequence, a perfect metallic contact between the top lid and the body is no longer required to avoid leakage [17], [22].

The RGW has been initially designed to operate between 17 GHz and 18 GHz (in K-band). This frequency range is chosen according to the RF power availability in the facility where MP validation tests will be performed, i.e., the High Power RF Space Laboratory of the European Space Agency (ESA) and the Val Space Consortium (VSC) [25]. Nevertheless, it is important to note that the validated MP study can be directly scaled up to higher frequency bands, where RGW is a very promising technological solution.

TABLE I
Standard SEY data for aluminium (Al) material

Material	E_{max} (eV)	E_1 (eV)	δ_0	δ_{max}
Al (ECSS2020 [27])	276.0	17.0	0.8	2.92

The selected initial dimensions must ensure a good frequency response, i.e., single-mode propagation from 17 GHz to 18 GHz, and a MP power level below 7 kW (maximum power level that can be measured in the cited laboratory). The simulations have been performed with the commercial software tool CST Studio Suite, (v. 2023, Dassault Systèmes) [26], which allows us to obtain the dispersion diagram and electromagnetic fields of the waveguide under study, and with SPARK3D (v. 2023, Dassault Systèmes). The latter one is a MP simulation tool that uses the computed electromagnetic fields in the component for driving charged particles (electrons). Taking into account the previous considerations, and after some iterations, we obtained the following initial RGW dimensions: a_{ridge} = 3 mm, h_{ridge} = 5.38 mm, $H_A = H_{gap}$ = 1.1 mm. Regarding the periodic bed of pins (of square cross-section with side a_{pin} and height h_{pin}, periodicity d and a separation p from the ridge to the first row of pins, see Fig. 1), it has been properly designed to implement the high-impedance surface required for the RGW technology, using the following dimensions p = 1.16 mm, d = 3.25 mm, a_{pin} = 1.5 mm, h_{pin}= 5.38 mm. Note that in this initial design, the same height has been chosen for both the ridge and pins, since in most existing designs using RGW, the height of the ridge is chosen to be identical to that of the pins for manufacturing simplicity.

The dispersion diagrams for this initial periodic bed of pins and the corresponding RGW are presented in Fig. 2, where Fig. 2(a) displays the dispersion diagram for the pin unit cell, and Fig. 2(b) shows the dispersion diagram for the RGW unit cell. In Fig. 2(b), the unwanted modes are depicted in blue, while the fundamental mode of the RGW is shown in red. The monomode operational bandwidth has been highlighted in grey, which ranges from approximately 11 GHz to 21 GHz.

Finally, we have performed the MP analysis of a finite section of this waveguide. The simulated results have been obtained for standard aluminum SEY data from [27], which are displayed in Table I. Fig. 3 shows the obtained MP power threshold P_{TH} of this RGW (h_{ridge} = 5.38 mm, H_{gap} = 1.1 mm) from 17 to 18 GHz. For the requested simulations, the driving EM fields have been computed with CST Studio Suite. Fig. 3 confirms that the initial RGW is suitable for performing MP measurements in the selected facility since the P_{TH} values are consistently below 6.8 kW, i.e., they remain within the 7 kW limit of the available laboratory equipment.

III. Relevance of the Study of MP Effect in the RGW

In this Section, we will first analyze the most relevant factors that can induce an electron discharge in the RGW. To this end, we will examine the region where EM fields are more intense in this waveguide, and hence, more susceptible for an electron discharge to occur.

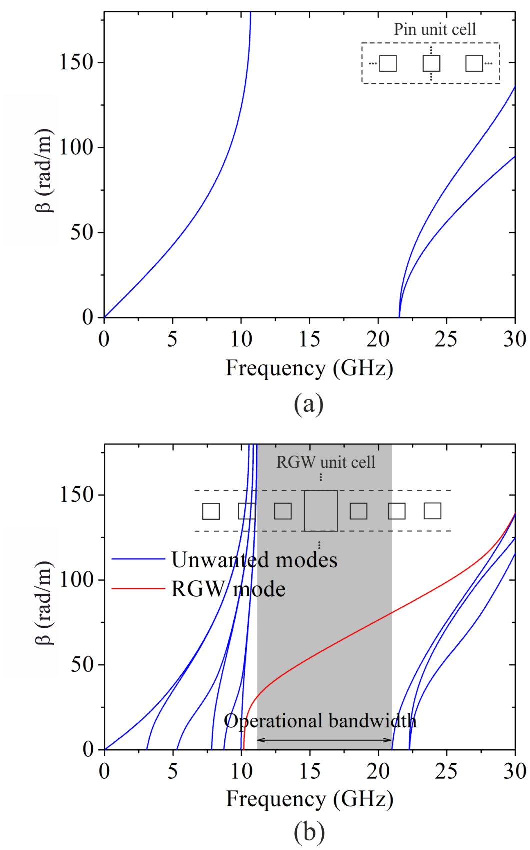

Fig. 2. Dispersion diagram of (a) the pin unit cell and (b) the RGW unit cell with the following parameters: a_{ridge} = 3 mm, h_{ridge} = 5.38 mm, H_A = H_{gap} = 1.1 mm, p = 1.16 mm, d = 3.25 mm, a_{pin} = 1.5 mm, h_{pin}= 5.38 mm.

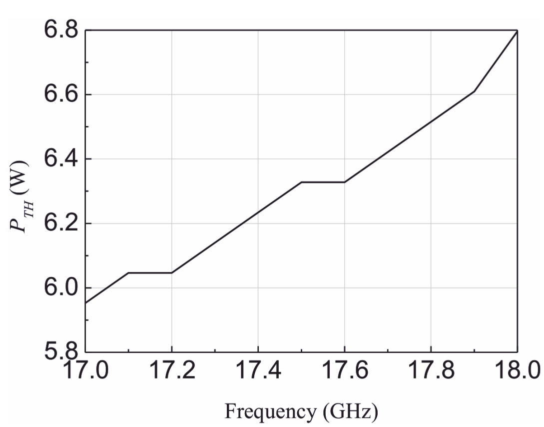

Fig. 3. P_{TH} computed with SPARK3D for a section of the initial RGW in the 17-18 GHz frequency range.

With this aim, the distribution of the electric field magnitude along the RGW geometry designed in Section II has been computed at 17.5 GHz, and it is shown in Fig. 4. For simplicity, ohmic losses have not been considered. As can be observed, the maximum field intensity is clearly located over the ridge. Given that MP is a voltage-driven effect, the ridge dimensions (its width a_{ridge} and height h_{ridge}), and especially the critical gap H_{gap} appearing in the RGW between the ridge and the top lid, are expected to be the most relevant factors that

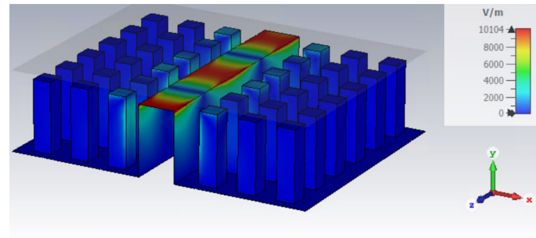

Fig. 4. Electric field distribution in the RGW of Fig. 2 at 17.5 GHz.

TABLE II
CHANGE OF THE CUTOFF FREQUENCY WITH THE RIDGE HEIGHT

Ridge height (mm)	5.38	5	3	2
f_c (GHz)	10.15	10.65	14.43	17.27

can influence the occurrence of an electron discharge in this waveguide. On the other hand, the fact that the field intensity is rather low in the metallic pins region (and much lower than in the ridge region in any case) also suggests that the pin parameters (their side a_{pin}, height h_{pin} and periodicity d) are unlikely to play a significant role in terms of MP effect in the RGW.

Furthermore, the effect of reducing the ridge height was investigated to understand its influence on the electromagnetic field distribution and the cutoff frequency. The results show that even with a reduced ridge height, the electromagnetic fields continue to be maximum over the ridge, unlike in the GGW case (where the electric field is more intense on the first row of pins [22]). Even when the cutoff frequency approaches the operating frequency of 17.5 GHz, the field still reaches its maximum over the ridge. This is shown in Fig. 5, where the ridge height is reduced to 3 mm. In Table II, the changes on the cutoff frequency from the reduction of the ridge height can be seen.

Next, a further investigation is performed about the P_{TH} levels in different waveguide technologies (including not only the RGW, which is the main subject of this work, but also other related waveguides as the GGW and the standard rectangular waveguide), in order to highlight the relevance of the MP study in the RGW in this work. At the same time, it will help us to evaluate the different techniques available to predict the P_{TH} in this waveguide, and to select the most suitable one for the subsequent parametric study of MP in the RGW. For comparison purposes, all results have been included in Table III. In this study we use the RGW designed in Section II, whose P_{TH} from 17 to 18 GHz calculated with SPARK3D was shown in Fig. 3, and listed at various frequency points in Table III. All SPARK3D simulations mentioned in this paper have been done with an initial homogeneously distributed electron volume of 10,000 electrons. In all cases, the whole volume of the design is imported to the simulation code, and no separate regions are created or studied.

In addition, we have estimated the P_{TH} in the RGW using the Critical Gap Voltage (CGV) prediction technique [30], in order to evaluate its suitability for the subsequent study to be performed in Section IV. This technique uses the peak

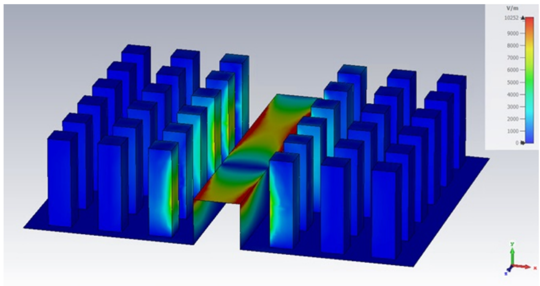

Fig. 5. Electric field distribution at 17.5 GHz in the RGW with h_{ridge}=3 mm.

voltage in the critical gap of the RGW for a continuous wave (CW) excitation at the waveguide input port of 1 W of mean power, V_{1W}, to predict the P_{TH} in this waveguide. The main benefit of this technique is the avoidance of the particle tracking simulation to obtain the prediction of the MP threshold. The drawback of this approach is the reduction of the accuracy, mainly due to the fact that the complete field spatial distribution inside the structure is not considered. Exploiting the fact that MP is a voltage-driven effect, the peak voltage V_{1W} inside the critical gap of the RGW (between the ridge and the top lid) can be computed using CST Studio Suite. For a matched waveguide section such as the analyzed RGW, this voltage is independent of the longitudinal position. However, the transverse position at which it is calculated must be carefully chosen, considering that the electromagnetic fields are not uniform above the ridge. In particular, we have checked that they are mainly concentrated above the ridge, having a maximum at the ridge center and decaying away from it, and although the electric field may have some singularity near the ridge corners, such areas are not relevant from a MP point of view due to the fringing-field effects [31] or random walk [32] that push electrons away from the ridge. This causes that a MP discharge cannot be sustained in the ridge corners, which is the reason why such areas are not considered for the calculation of the peak voltage V_{1W}. Thus, it must then be computed at the ridge center, for an input power of 1 W. V_{1W} can then be combined with the peak threshold voltage required for a discharge on such gap, V_{TH} (which can be obtained from the PPW susceptibility charts), to predict the P_{TH} in our RGW using the well-known relationship [30]:

$$P_{TH} = P_{1W} \ (\frac{V_{TH}}{V_{1W}})^2 = 1W \ (\frac{V_{TH}}{V_{1W}})^2 \tag{1}$$

For comparative purposes, the resulting P_{TH} values obtained with the CGV technique for the RGW have also been included in Table III. In such table, it can be seen considerably lower results than the calculated ones with SPARK3D, mainly related to the use of the peak threshold voltage V_{TH} from the PPW susceptibility chart, as the parallel-plate case is the geometry providing the lowest MP threshold (due to the lack of fringing-field effects pushing electrons away from the critical gap [31] or random walk [32]).

We have also compared the previously obtained P_{TH} level in our RGW with that of a section of an equivalent Ridge Rectangular Waveguide (RRW) of the same length with SPARK3D, i.e. with perfect vertical electric walls instead of the bed of pins, with the same ridge dimensions (a_{ridge} = 3 mm, h_{ridge} = 5.38 mm, and with the equivalent waveguide dimensions ($a_{RRW} = 2p + a_{ridge} = 5.32$ mm, $b_{RRW} = 6.477$ mm), whose results are included in Table III, showing slightly higher P_{TH} values in the RRW, due to the electric-field distribution.

TABLE III
COMPARISON OF P_{TH} IN DIFFERENT WAVEGUIDE TECHNOLOGIES IN THE 17-18 GHZ FREQUENCY BAND

Waveguide technology	GAP (mm)	P_{TH} (kW) at 17 GHz	P_{TH} (kW) at 17.5 GHz	P_{TH} (kW) at 18 GHz
RGW of Fig. 2 SPARK3D	1.1	5.953	6.328	6.797
RGW of Fig. 2 CGV prediction	1.1	4.837	5.156	5.496
RRW SPARK3D	1.1	6.262	6.662	7.162
WR-51 RW SPARK3D	6.477	110.0	121.0	132.0
RW [24] $b = 3$ mm	3.0	18.6	20.45	22.0
GGW [24] $b = 3$ mm	3.0	20.9	22.4	24.4

Next, for comparison purposes, we have also studied the P_{TH} level in other related waveguide technologies susceptible to electron discharge. In particular, we will compare the previously P_{TH} level obtained in the studied RGW, within the 17-18 frequency band, with the P_{TH} obtained in two different RWs.

Firstly, we have computed the P_{TH} values in a standard WR-51 RW (with dimensions $a_{WR-51} = 12.954$ mm, $b_{WR-51} = 6.477$ mm), and also in the same WR-51 RW with a reduced height of $b_{WR-51} = 3$ mm, which has been studied in [24]. The P_{TH} values (obtained with SPARK3D, and using the same SEY [27] for the waveguide surfaces as in the RGW) have been included in Table III. In both cases, significantly higher values have been obtained than in the RGW case. This can be easily understood, given that the critical gap in the RGW is much smaller, so the V_{TH} (and P_{TH}) level for an electron discharge to occur in the RGW will be much lower, thus highlighting the relevance of the study of MP in the RGW.

Finally, we have also studied the P_{TH} in GGW technology. To this end, we show the P_{TH} in the corresponding GGW counterpart of the previously analyzed WR-51 RW with reduced height of $b_{WR-51} = 3$ mm also studied in [24], and whose bed of pins parameters are detailed in such reference. In this GGW, the gap H_A between the pins and the top lid has been ideally set to 0 μm, corresponding to the zero-gap approximation, in order to avoid undesired MP discharges that, as thoroughly studied in uniform GGW sections [22], can be easily triggered at very low power levels in the air gaps of the classical GGW case. The calculated P_{TH} values of this GGW at different frequencies, obtained with SPARK3D, and using the same SEY [27] for the waveguide surfaces as in the RGW, are also included in Table III. It can be seen that values for the GGW case are slightly higher than those obtained in its RW counterpart in all frequencies considered, as already found in [22], and above all, significantly higher than in the RGW, highlighting once again the relevance of the MP study in the RGW.

IV. Parametric study of MP in the RGW

In this Section, starting from the initial RGW designed in Section II, and in order to know the sensitivity of this RGW in terms of MP breakdown to variations in its geometry, a complete parametric study has been carried out. Given that MP depends on the impact energy being between certain values and a synchronism condition, in all the performed MP analyses, the complete structure including the pins has been always simulated with Spark3D, and in all the presented results we have always checked that the electron discharge occurs over the ridge and not over the pins. This can be easily predicted for the case of a RGW with the same height for both the ridge and pins (and thus with the same gap). However, we checked by means of simulations that this is no longer true for lower ridge height values, which limited our parametric study in terms of the ridge height to a minimum value of 4 mm, as will be shown next. In any case, it is important to emphasize that, in practice, in most existing ridge gap waveguide designs the ridge and the pins are manufactured with the same height, and we can state that in such cases, regardless of the gap size, the MP discharge always occurs on the ridge and not on the pins.

In the analysis performed in Section III, it has been concluded that the most relevant parameters to be studied in this waveguide, in terms of MP breakdown, are the ridge width a_{ridge} and height h_{ridge}, and also the distance between the ridge and the bed of pins p. However, the parameters of the periodic bed of pins are not relevant in the RGW in terms of MP effect, given that even with a reduced ridge height, the maximum electromagnetic field in the RGW remains over the ridge and not in the pins region, unlike in the GGW case [22]. Thus, we have performed an analysis of the obtained MP power threshold P_{TH} of such waveguide when varying its fundamental design parameters (the ridge width a_{ridge} and ridge height h_{ridge}, and also the distance between the ridge and the bed of pins, see Fig. 1) at the frequency of 17.5 GHz. Regarding their range of variation, they have been limited by a proper monomode waveguide operation in the considered frequency range (from 17 to 18 GHz).

Figure 6 shows the calculated MP power threshold P_{TH} levels in the RGW as a function of the ridge width a_{ridge}, which has been varied from 3 to 5 mm. In the same figure, we have also shown the P_{TH} levels when varying the ridge height h_{ridge} from 4 to 5.38 mm (each curve corresponds to a different ridge height). The distance from the ridge to the bed of pins is kept constant at p = 1.16 mm, as in the initial design. The parametric study of the dependence of the P_{TH} with the ridge parameters reveals that the ridge height of the RGW has a significant impact on the threshold power required for a MP electron discharge to occur, as can be seen in Fig. 6. This result was already anticipated in the previous Section, given that this parameter is directly related to the larger or smaller gap that exists in the region where the electromagnetic field is more intense. Specifically, the higher the ridge height, the smaller the gap between the ridge and the top metal lid, so a lower power is required for an electron discharge to occur in the RGW. On the other hand, as the ridge width increases, it is observed that the threshold power remains relatively stable for most cases, with a slight increasing trend observed for the shorter ridge value when h_{ridge}=4 mm. These observations suggest that the ridge width will not be a critical parameter in terms of threshold power, while the ridge height will play a determining role.

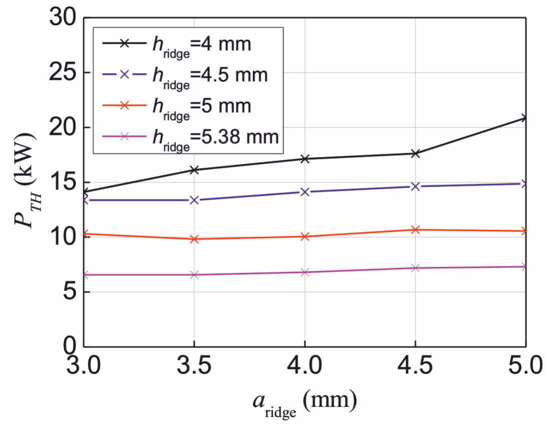

Fig. 6. P_{TH},as a function of a_{ridge} for different values of h_{ridge}.

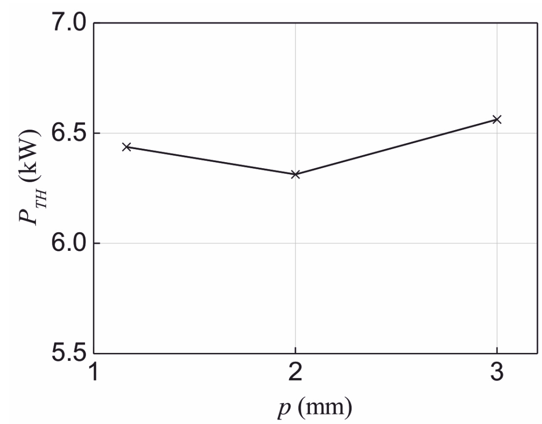

Fig. 7. P_{TH} depending on distance between the ridge and the bed of pins.

Furthermore, we have studied the behavior of the RGW in terms of P_{TH} when varying the distance between the bed of pins and the central ridge p, which has been varied from 1.16 to 3 mm, while keeping the remaining parameters equal to those in the initial RGW configuration. The results shown in Fig. 7 indicate that the distance between the central ridge and the bed of pins is not a relevant parameter in terms of the threshold power the RGW can support, as only minor variations were observed between different values of this distance. It is important to note that, for all analyzed cases, the MP discharge occurred in the central area over the ridge.

The most important conclusions to highlight about the performed parametric study can be summarized as follows: the ridge width is not a relevant factor in terms of the MP threshold power of the RGW. This allows for a good margin and degree of freedom when designing a RGW. It is important to remember that this is a key factor in components designs, as the variation of the width is usually employed to control the characteristic impedance of the line. As with the width, the distance between the central ridge and the bed of pins (p) has minimal impact on the MP threshold power level it can support, even for significant variations of this p parameter. This insensitivity is advantageous for practical designs involving bends or corners, where maintaining a constant distance between the pins and the ridge is not always feasible. In contrast, the ridge height is the most critical parameter in terms of power handling in the design of a RGW. It has a direct and nearly inverse relationship with the MP threshold power: the higher the ridge height, the lower the threshold power. This is because increasing the ridge height reduces the gap between the ridge and the top lid, making the structure more susceptible to an electron discharge in this area.

V. Transformer Design

All the conclusions extracted in the previous Section have been obtained based on theoretical considerations, and simulations performed in the selected RGW through electromagnetic field computations, and MP modeling software using perfect conductor material (thus minimizing insertion losses). Now, in order to fully validate these results, a RGW prototype has been designed and manufactured, and its electrical response has been measured and the corresponding MP test has been completed.

To perform MP tests in the available high power laboratory, the designed RGW will need to be connected to standard rectangular waveguide ports. Hence, it is essential to design a matching stage, consisting of an impedance transformer from the standard waveguide to the designed RGW.

In particular, as the MP tests of the RGW prototype will be done in the frequency band of 17-18 GHz, the standard $WR-51$ will be used in the laboratory as a waveguide port, whose monomode operation frequency range is located between 15 and 22 GHz. On the other hand, given that at the operating frequency band of 17-18 GHz the maximum measurable power in the laboratory is about 6.5 - 7 kW, the transformer has been designed for a RGW with the following parameters: a_{ridge} = 3 mm, $h_{ridge} = h_{pin}$ = 5.75 mm, H_{gap} = 0.727 mm (with the rest of pin parameters as indicated in Fig. 2). These values correspond to the final ridge dimensions, where the ridge height has been increased compared to the previous analysis (from 5.38 mm to 5.75 mm). This adjustment was made after verifying the P_{TH} results and considering the maximum power available in the laboratory, as a way to ensure that the MP threshold could be experimentally measured within the accessible power range. Increasing the ridge height, the MP threshold decreases, and we guarantee that the power level can be measured. It is also important to note that after including the impedance transformer, the P_{TH} levels may be slightly modified if an optimal electrical response is not finally achieved, which will be checked next.

The impedance transformer will consist of a series of consecutive ridge steps made in gap waveguide technology, whose ridge width gradually decreases while the height increases, since the standard $WR-51$ waveguide is significantly wider

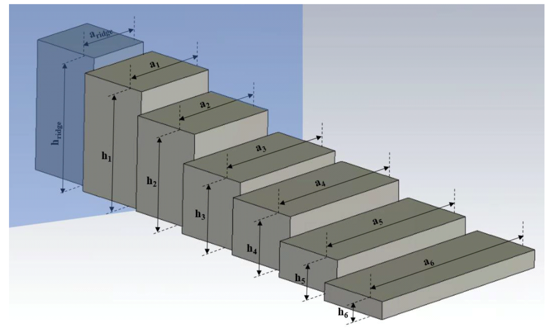

Fig. 8. Scheme of one half of the designed transformer (without the bed of pins) with the ridge height and width dimensions.

TABLE IV
Steps Height and Width in the Designed Transformer

a_1	a_2	a_3	a_4	a_5	a_6
4.02	4.37	5.53	6.62	7.57	9.51
b_1	b_2	b_3	b_4	b_5	b_6
5.21	4.25	3.04	2.45	1.54	0.85

than the designed RGW and lacks a ridge in its cross-section. Therefore, as shown in the schematic of one half of the designed transformer in Fig. 8 (where the bed of pins is not shown for simplicity), we start with an initial ridge block that is nearly as wide as the $WR-51$ and has a small height. The following blocks gradually decrease in width and increase in height ending with a final block whose ridge dimensions are very close to the height and width of the designed RGW ridge.

Our impedance transformer will be based on an initial model of 7 steps progressively decreasing from the initial ridge of our RGW (in blue in Fig. 8) to the standard $WR-51$ waveguide (with no ridge and thus not shown). The dimensions of the 6 intermediate ridges are given in Fig. 8. These final values for matching a section of RGW of 6 periodic cells (i.e. with 6 metallic pins along the propagation direction) are given in Table IV- They have been determined after an optimization process performed in CST Studio Suite.

Fig. 9 shows the description of the complete RGW to $WR-51$ waveguide transformer with the central section of the designed RGW. Its simulated S-parameters are presented in Fig. 10 (here metal losses of aluminium have been considered). Although the RGW has been specifically designed for operation in the 17-18 GHz frequency band, the RGW to $WR-51$ waveguide transformer has been optimized for a wider frequency band, which extends from 15.5 to 20.5 GHz. Within that band, the return losses are higher than 20 dB, and the insertion losses in a back to back configuration are lower than 2 dB, thus revealing a very good matching between both waveguides (see simulated results in Fig. 10).

Once the final prototype of the impedance transformer has been designed and electromagnetically characterized, its high-power study was carried out using SPARK3D to evaluate its MP behavior. In order to simulate the MP effect more realistically, in addition to using the SEY standard data for the material involved (aluminium) [27], as is usually done (see Sections II and IV), measured results for such key material

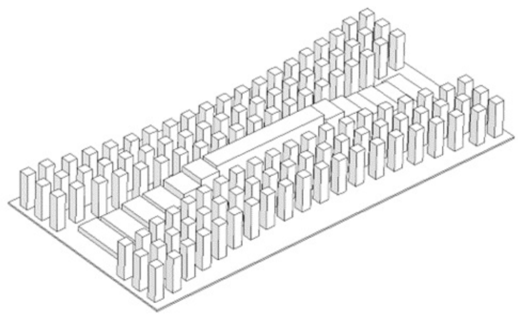

Fig. 9. 3-D view of the transformer with the RGW central section.

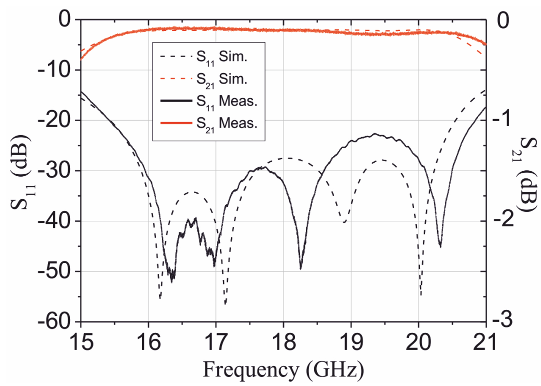

Fig. 10. Simulated and measured S-parameters of the RGW transformer.

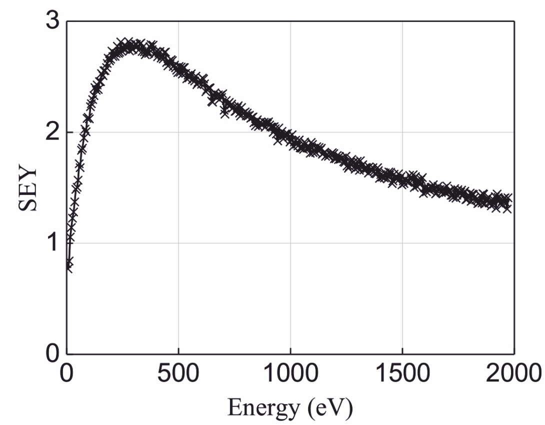

Fig. 11. Experimental SEY measured at the European High Power Space Materials Laboratory [25].

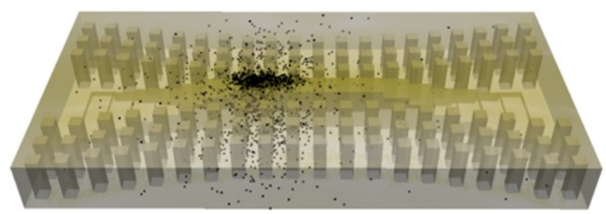

Fig. 12. Electron cloud distribution of a MP discharge (RF input power of 4.3 kW at 17 GHz) inside the transformer.

property will be employed in this Section. To this aim, the corresponding experimental SEY data have been obtained from the metallic top lid of the fabricated transformer through measurements performed at the European High Power Space Materials Laboratory [25]. These measured values for the real aluminium sample are shown in Fig. 11, and will be used next.

Following the MP analysis in the designed transformer, all the high-power simulations (using the obtained experimental SEY data displayed in Fig. 11) have shown that the discharge electron clouds are always located in the RGW (central area of the transformer) and above the ridge (see, for example, the electron cloud distribution shown in Fig. 12 for an RF input power of 4.3 kW at 17 GHz). The calculated P_{TH} values in the designed RGW with and without the transformers (back-to-back configuration) are represented in Fig. 13. The P_{TH} levels are similar across the analyzed frequency range, indicating that the field intensity in the RGW section is nearly the same in both structures (with and without transformer sections). This behavior is consistent with the good simulated electrical performance of the designed transformer, as shown in Fig. 10, which exhibits high return losses and low insertion losses. These values are below the maximum power that can be measured in the laboratory (about 6.5 - 7 kW) for the considered frequency range, as expected from the previous MP analysis performed on this RGW without the transformers.

VI. Fabrication and Experimental Results

A prototype of the designed RGW, which includes transformers with a back-to-back configuration, has been manufactured in aluminium employing a computer numerical control (CNC) milling technique (shown in Fig. 14). Before any experimental measurement is carried out, all parts, including the metal lid, bolts, washers and nuts, were washed in an ultrasonic bath (2-propanol). After that, the transformer with the RGW design was assembled.

The measured frequency response of the fabricated prototype is represented in Fig. 10 (solid line), along with the simulation results (dashed line). Overall, there is a good correlation between the two sets of data. Some minor discrepancies are noticeable in the 18.5 to 20 GHz range, where the measured return losses are slightly lower. This behavior is attributed to small manufacturing variations, which are not unusual for these high-frequency components. However, considering that the experimental MP study is conducted in the 17-18 GHz frequency range, it can be concluded that the performance of the manufactured transformer meets the required specifications (in terms of both IL and RL levels) to perform the high-power tests in the selected experimental facility.

As indicated before, the MP experimental campaign has been performed at the High Power RF Space Laboratory of ESA and VSC [25], where all the necessary equipment (in particular, power amplifiers up to Ka-band frequency range) is available. The campaign was carried out in a class 10,000 (ISO7) certified clean room. The nominal temperature of the clean room is 22°C (plus/minus 1°C). The hardware was handled and stored following flight model (FM) precautions.

A standard experimental setup (according to [28]) was assembled to perform the MP measurements of the manufactured prototype, with the parameters provided in Table V. This setup delivers up to 6 kW peak power.

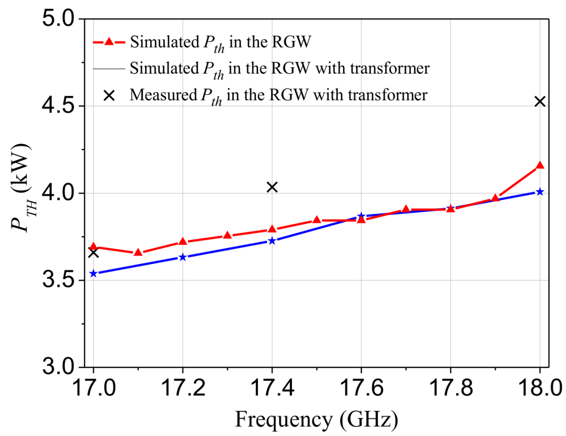

Fig. 13. Simulated and measured P_{TH} in the designed RGW including transformers (back-to-back configuration). The obtained P_{TH} in the designed RGW without the transformers is also included for comparison.

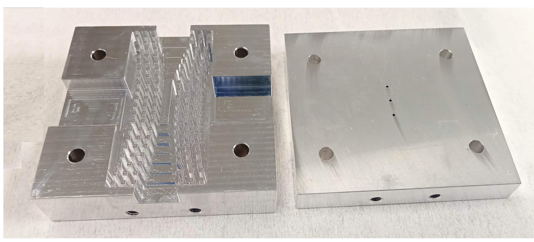

Fig. 14. View of the manufactured transformer (body -left- and top -right-).

TABLE V
MULTIPACTOR TEST PARAMETERS

Parameter	Value
Multipactor tests Frequency	17 GHz, 17.4 GHz and 18 GHz
Max. RF power	6 kWpk
Signal length	20 µs
Duty cycle	2%
Pressure	$\leq 1 \cdot 10^{-5}$ mbar
Test temperature	+23 °C
Bake-out temperature	+85 °C for 12 h
Electron seeding	βSr^{90} source

Before starting vacuum-based tests, an ambient pressure test (APT) is performed in the thermal vacuum chamber (TVAC, see Fig. 15), after which the vacuum system begins the evacuation cycle, followed by bake-out steps before each test.

In order to simulate the space environment and initiate the MP effect, a radioactive $Sr^{90}\beta$ source was used as an electron seeding mechanism. During each test, critical parameters, including the temperature at several points on the DUT, the applied and reflected RF power, and the system losses, were continuously monitored.

RF discharges were detected using both global and local methods. Global techniques included phase-nulling and third-harmonic detection systems [28], which are particularly effective for single-tone CW signals. In parallel, electrometers (which detect the growth of the electron population in the vicinity of critical areas of the samples) were placed near sensitive regions of the structure to detect local electron accumulation. The $Sr^{90}\beta$ source was directed at the central

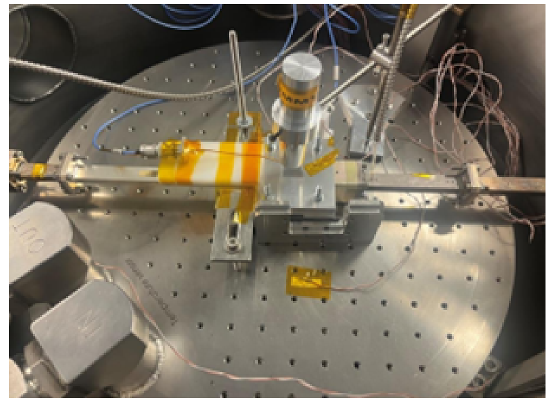

Fig. 15. Internal view of the thermal vacuum chamber with the prototype.

part of the RGW region, where higher electromagnetic fields were expected to appear.

Fig. 13 presents a comparison of the simulated MP threshold power levels, obtained using SPARK3D and considering the experimental SEY of aluminum, for configurations with and without transformer sections, and the experimentally measured data acquired under Sr^{90} exposure at three frequency values (17, 17.4, and 18 GHz).

The simulation results predict very well the measured breakdown power at 17 GHz, although the breakdown power levels detected at 17.4 and 18 GHz are slightly higher than the simulated ones. In real materials, even minor deviations in SEY can noticeably shift MP levels, even beyond the difference observed in Fig. 13. We verified through simulations that a reduction of the SEY measured values shown in Fig. 11 in a value of 0.06 leads to simulated P_{TH} values that match the experimental results. Such small variations in SEY may occur due to aging or surface contamination effects. Thus, the small difference observed around 300 W between the simulated and measured levels of P_{TH} allows us to validate the MP study in RGWs performed in this work.

VII. CONCLUSION

In this work, a theoretical and experimental study of the MP effect in RGW technology has been performed. To this aim, simulated results (using a commercial software tool) of the dependence of MP power threshold on various parameters, such as the ridge dimensions and its proximity to the bed of pins is considered.

The study reveals that, in terms of power handling, the most relevant parameter in the RGW under study is the ridge height. The higher the ridge height, the lower the MP threshold power that supports the RGW. On the other hand, the rest of RGW parameters (the ridge width, the distance from the ridge to the bed of pins and the pins parameters) are not relevant in terms of the MP threshold power of the RGW, and therefore we can afford a good margin and degree of freedom when designing a RGW.

These conclusions are relevant for practical designs, as it is common practice when designing devices with RGW to adjust the ridge width to achieve different impedances, while the distance to the bed of pins is not always kept constant due to bends or corners present in most components. Therefore, the insensitivity of the MP threshold to these two parameters is important for microwave engineers. However, the dependence on ridge height is a factor that must be taken into account. In most existing designs, the ridge height is assumed to be identical to the height of the surrounding pins to simplify the manufacturing process. However, the gap between the pins and the top lid is typically kept quite small to increase the bandgap provided by the pins, which can compromise the MP threshold. In principle, the ridge height can be chosen to be lower than that of the pins without affecting waveguide performance. Thus, the conclusions from this study are crucial to be considered when addressing space-related applications, using this novel guided technology.

For validation purposes, a RGW transformer has been successfully designed and manufactured, and it has been confirmed that potential RF discharges can only occur in the central section of the RGW transformer under study. Experimental results (of both electrical responses and high vacuum RF discharges) fully confirm all previously simulated results, as well as the good performance of the RGW technology in terms of the MP effect.

VIII. Acknowledgments

The authors would like to thank Nelson Castro for his collaboration in this work, and the European High Power RF Space Laboratory of the European Space Agency and Val Space Consortium for contributing with its installations – Laboratory co-funded by the European Regional Development Fund – A way of making Europe.

References

[1] J. R. M. Vaughan, “Multipactor,” *IEEE Trans. Electron Devices*, vol. ED-35, no. 7, pp. 1172–1180, Jul. 1988.

[2] M. Jiménez, B. Gimeno, C. Miquel-Espanya, D. Raboso, S. Anza, C. Vicente, J. Gil, F. Quesada, Á. Alvarez, M. Taroncher, M. Reglero, V.E. Boria, “Analysis of the electromagnetic radiation generated by a multipactor discharge occurring within a microwave passive component,” *J. Phys. D: Appl. Phys*, vol. 43, no. 39, p. 395501, Oct. 2010.

[3] A. J. Hatch and H. B. Williams, “The secondary electron resonance mechanism of low-pressure high-frequency gas breakdown,” *J. Appl. Phys.*, vol. 25, no. 4, pp. 417–423, Apr. 1954.

[4] A. Wood and J. Petit, “Diagnostic investigations into the multipactor effect, susceptibility zone measurements and parameters affecting a discharge,” *ESA/ESTEC*, Noordwijk, The Netherlands, Work. Paper 1556, Nov. 1989.

[5] A. Coves, G. Torregrosa-Penalva, C. P. Vicente, A. M. Pérez, B. Gimeno, and V. E. Boria, “Time evolution of an electron discharge in a parallel-plate dielectric-loaded waveguide,” *IEEE Trans. Electron Devices*, vol. 55, no. 9, pp. 2505–2511, Sep. 2008.

[6] G. Torregrosa-Penalva, A. Coves, B. Gimeno, I. Montero, C. Vicente, and V. E. Boria, “Multipactor susceptibility charts of a parallel-plate dielectric-loaded waveguide,” *IEEE Trans. Electron Devices*, vol. 57, no. 5, pp. 1160–1166, May. 2010.

[7] V. E. Semenov, E. I. Rakova, D. Anderson, M. Lisak, and J. Puech, “Multipactor in rectangular waveguides,” *Phys. Plasmas*, vol. 14, no. 3, p. 033501, Mar. 2007.

[8] A. Berenguer, Á. Coves, F. Mesa, E. Bronchalo, and B. Gimeno, “Analysis of multipactor effect in a partially dielectric-loaded rectangular waveguide,” *IEEE Trans. Plasma Sci.,*, vol. 47, no. 1, pp. 2687–2697, Jan. 2019.

[9] P. Soto, D. de Llanos, V. E. Boria, E. Tarín, B. Gimeno, A. Oñoro, I. Hidalgo, and M. J. Padilla, “Performance analysis and comparison of symmetrical and asymmetrical configurations of evanescent mode ridge waveguide filters,” *Radio Science,*, vol. 44, no. 06, pp. 1–16, 2009.

[10] D. Gonzalez-Iglesias, P. Soto, S. Anza, B. Gimeno, V. E. Boria, C. Vicente, and J. Gil, “Multipactor susceptibility charts for ridge and multiridge waveguides,” *IEEE Trans. Electron Devices*, vol. 59, no. 12, pp. 3601–3607, 2012.

[11] A. M. Pérez, V. E. Boria, B. Gimeno, S. Anza, C. Vicente, and J. Gil, “Multipactor analysis in circular waveguides,” *J. Electromagn. Waves Appl.*, vol. 23, no. 11—12, pp. 1575–1583, 2009.

[12] A. Frotanpour, B. Gimeno, and S. Esfandiarpour, “Multipactor in dualmode elliptical waveguide,” in *Proc. 31st Int. Rev. Prog. Appl.Comput. Electromagn.*, (ACES), Williamsburg, VA, USA, May 2015, pp. 1–2.

[13] A. M. Pérez, V.E. Boria, C. Tienda, C. Vicente, S. Anza, J. Gil, B. Gimeno, and D. Raboso, “Prediction of multipactor breakdown thresholds in coaxial transmission lines for traveling, standing, and mixed waves,” *IEEE Trans. Plasma Sci.*, vol. 37, no. 10, pp. 2031–2040, Oct. 2009.

[14] D. González-Iglesias, O. Monerris, B. G. Martínez, M. E. Díaz, V. E. Boria, and P. Martín-Iglesias, “Multipactor RF breakdown in coaxial transmission lines with digitally modulated signals,” *IEEE Trans. Electron Devices*, vol. 63, no. 10, pp. 4096–4103, Oct. 2016.

[15] V. E. Semenov, E. I. Rakova, A. G. Sazontov, I. M. Nefedov, V. I. Pozdnyakova, I. A. Shereshevskii, D. Anderson, M. Lisak, and J. Puech, “Simulations of multipactor thresholds in shielded microstrip lines,” *J. Phys. D: Appl. Phys.*, vol. 42, no. 20, p. 205204, Sep. 2009.

[16] P. S. Kildal, E. Alfonso, A. Valero-Nogueira and E. Rajo-Iglesias, “Local metamaterial-based waveguides in gaps between parallel metal plates,” *IEEE Antennas and Wireless Propagation Letters*, vol. 8, pp. 84–87, 2009.

[17] E. Rajo-Iglesias and P. S. Kildal, “Numerical studies of bandwidth of parallel-plate cut-off realised by a bed of nails, corrugations and mushroom-type electromagnetic bandgap for use in gap waveguides,” *IET Microw. Antennas Propag.*, vol. 5, no. 3, p. 282–289, Feb. 2011.

[18] P. Kildal, A. Zaman, and E. Rajo-Iglesias, “Design and experimental verification of ridge gap waveguides in bed of nails for parallel plate mode suppression,” *IET Microw. Antennas Propagat.*, vol. 5, no. 3, pp. 262–270, Feb. 2011.

[19] E. Alfonso, M. Baquero, P. Kildal, A. Valero-Nogueira, E. Rajo-Iglesias and J. I. Herranz, “Design of microwave circuits in ridge-gap waveguide technology,” in *Proc. 2010 IEEE MTT-S International Microwave Symposium*, Anaheim, CA, USA, 2010, pp. 1–1.

[20] E. Rajo-Iglesias, M. Ferrando-Rocher and A. U. Zaman, “Gap waveguide technology for millimeter-wave antenna systems,” *IEEE Communications Magazine*, vol. 56, no. 7, pp. 14–20, Jul. 2018.

[21] A. Farahbakhsh, D. Zarifi, and A. U. Zaman, “A mmWave wideband slot array antenna based on ridge gap waveguide with 30% bandwidth,” *IEEE Trans. Antennas Propagat.*, vol. 66, no. 2, pp. 1008–1013, Feb. 2018.

[22] J. J. Vague, I. Asensio, Á. Coves, Á. A. San Blas, M. Reglero, A. Vidal, D. Raboso, M. Baquero-Escudero, and V. E. Boria, “Study of the multipactor effect in groove gap waveguide technology,” *IEEE Trans. Microw. Theory Techn.*, vol.70, no. 5, pp. 2566–2578, May 2022.

[23] A. Morales-Hernández, M. Á. Sánchez-Soriano, M. Ferrando-Rocher, S. Marini, and V. E. Boria, “In-depth study of the corona discharge breakdown thresholds in groove gapwaveguides and enhancement strategies for inductive bandpass filters,” *IEEE Access*, vol.10, pp. 129149—129162, 2022.

[24] A. Jorge-López, J. J. Vague, I. Asensio, A. Coves, A. A. San-Blas, M. Baquero-Escudero, M. Taroncher, A. Vidal, and V. E. Boria, “Theoretical and Experimental Results for Multipactor Effect in Groove Gap Waveguide Bandpass Filters With Inductive Coupling Irises,” *IEEE Access*, vol.12, pp. 187844–187856, 2024.

[25] European Space Agency (ESA) and Val Space Consortium (VSC) High-Power Laboratories, Valencia, Spain. [Online]. Available: www.val-space.com

[26] CST Studio Suite, version 2023, Dassault Systèmes, 2023.

[27] “Multipacting and Design Test,” European Cooperation for Space Standarization (ECSS), ESA-ESTEC, ESA Publication Division, The Netherlands, Rep. ECSS-E-ST-20-01C, Jun. 2020.

[28] “Multipacting Handbook,” European Cooperation for Space Standarization (ECSS), ESA-ESTEC, ESA Publication Division, Amsterdam, The Netherlands, Rep. ECSS-E-HB-20-01A, Jun. 2020.

[29] ECSS multipactor tool. Available at http://www.val-space.com/highpowerlabrf/multipactor-tool/, accessed 1 September 2025.

[30] P. Gonzalez, C. Alcaide, R. Cervera, M. Rodríguez, O. Monerris, J. Petit, A. Rodríguez, A. Vidal, J. Vague, J.V. Morro, P. Soto, and V.E. Boria, ”Multipactor threshold estimation techniques based on circuit models electromagnetic fields and particle simulators”, *IEEE J. Microw.*, vol. 2, no. 1, pp. 57-77, Jan. 2022.

[31] A. Al-Mudhafar, J. Puech, and H. Hartnagel, “Investigation of multipactor effect in microwave components in the presence of fringing fields,” in *Proc. IEEE 44th Eur. Microw. Conf.*, Rome, Italy, Oct. 2014, pp. 406–409.

[32] V. E. Semenov, E. Rakova, R. Udiljak, D. Anderson, M. Lisak, and J. Puech, “Conformal mapping analysis of multipactor breakdown in waveguide irises,” *Phys. Plasmas*, vol. 15, no. 3, p. 033501, Mar. 2007.